Tunable Filtering of Orbital Angular Momentum Modes via Spatial Depth-Dependent Mode Transformation

Haisheng Wu(吴海生)[1†], Huihua Huang(黄辉华)[1†], Shu Chen(陈舒)[1†], Jing Wang(王晶)[1], Qingji Zeng(曾庆计)[1], Bowei Zhang(张博维)[1], Junmin Liu(刘俊敏)[2], Huapeng Ye(叶华朋)[3], Ze Dong(董泽)[4], Dianyuan Fan(范滇元)[1*], and Shuqing Chen(陈书青)[1*]

[1]*Institute of Microscale Optoelectronics, Shenzhen University, Shenzhen 518000, China*
[2]*College of New Materials and New Energies, Shenzhen Technology University, Shenzhen 518118, China*
[3]*School of Information and Electronics, Beijing Institute of Technology, Beijing 100081, China*
[4]*South China Academy of Advanced Optoelectronics, South China Normal University, Guangzhou 510006, China*

(Received 8 September 2024; accepted manuscript online 22 November 2024)

Advancements in orbital angular momentum (OAM) mode-multiplexing communication networks require tunable mode filters for selective channel demultiplexing and downloading. In this study, we propose a spatial depth-dependent mode transformation strategy for the tunable filtering of OAM modes. By integrating the spiral phase and lens phase modulations, we achieved mode conversions that varied with the transmission depth, enabling selective demultiplexing in predetermined axial planes. This approach facilitates tunable mode filtering by adjusting spatial depths. As a proof of concept, we fabricated a mode filter using two-photon polymerization lithography (TPL) technology, successfully filtering five OAM modes with mode crosstalk below −10.9 dB. Additionally, the filter was applied in a mode-multiplexing communication link, achieving tunable demultiplexing of five mode channels with bit error rates below 10^{-6}. These results highlight the efficacy and flexibility of our strategy for OAM mode filtering and offer promising insights for the development of mode-multiplexing communication networks and channel interconnections.

DOI: 10.1088/0256-307X/41/12/124203

Owing to their inherent mode orthogonality, vortex beams carrying orbital angular momentum (OAM) modes[1,2] have demonstrated substantial potential for enhancing the capacity density of optical communications and constructing robust communication networks. Various mode (de)multiplexing[3–5] technologies, including forked gratings[6,7] and angular lenses,[8,9] have been extensively explored to increase communication capabilities. To facilitate the development of communication networks and achieve channel interconnections, the advancement of tunable mode filtering technology is essential for selective demultiplexing and channel downloading at the network nodes. By leveraging the rotational symmetry of spiral-phase wavefronts, Mach–Zehnder interference[10–12] can separate two OAM modes into different transmission directions via constructive and destructive self-interference. However, manipulating multiple modes requires the cascading of several interferometer systems, leading to increased system redundancy and mode crosstalk. To mitigate these challenges, optical geometric transforms[13–15] have been proposed to separate the coaxial OAM modes into distinct transverse positions. Nevertheless, these approaches are limited to mapping modes to fixed spatial positions, which fails to satisfy the need for the selective separation of OAM modes. Furthermore, as the number of modes increases, the reduced separation distances cause a significant overlap of the optical spots, complicating the extraction of subsequent modes. Therefore, there is an urgent need to explore effective and tunable mode-separation strategies to overcome mode crosstalk in mode filtering and provide flexible modulation capabilities.[16]

In this paper, we propose a spatial depth-dependent mode transformation strategy to map OAM modes to distinct spatial depths for tunable filtering. The mode-independent nature of spatiotemporal evolution allows the continuous modulation of incident spatial modes during light transmission,[17] thereby facilitating depth-dependent mode transformations in free space. This linear relationship between depth and mode enables the precise mapping of mode information to different depth planes,[18] with potential applications in depth-multiplexing holography,[19–21] optical encryption,[22,23] and the spatial engineering of structured light modes.[24–26] By integrating the spiral and lens phase modulations, we achieved mode conversions that varied with transmission distance. By leveraging the conservation of OAM, multiplexed modes can be independently demultiplexed and separated at predetermined depth planes,[27] allowing selective mode filtering by adjusting the transmission depth. Furthermore, the inherent divergence difference between the filtered modes enhances their mutual separation, ensuring low mode crosstalk during the filter-

†These authors contributed equally to this work.
*Corresponding author. Email: shuqingchen@szu.edu.cn; fandy@cae.cn
© 2024 Chinese Physical Society and IOP Publishing Ltd

ing process. Thus, the introduction of a spatial depth-dependent mode transformation provides an effective solution for tunable mode separation and filtering.

By utilizing spatial depth-dependent mode transformation in conjunction with two-photon polymerization lithography (TPL), we designed and fabricated a mode filter for selective mode demultiplexing. In our experiments, we demonstrated tunable filtering of five OAM modes by adjusting the transmission depths from 13.5 to 39 mm, achieving an average mode crosstalk below −10.9 dBm. Additionally, we constructed a five-channel OAM mode-multiplexing communication link, with each channel transmitting 50 Gbit/s quadrature-phase shift-keying (QPSK) signals. Using the proposed mode filter, all channels were selectively demultiplexed, achieving bit error rates (BERs) below 1×10^{-6} at a received optical power of −16 dBm. We further explored the flexibility of this approach by extending the spatial depth range and incorporating angle dimensions, demonstrating that additional mode channels can be downloaded at various spatial positions. This method has significant potential for accommodating a large number of mode-multiplexing channels.

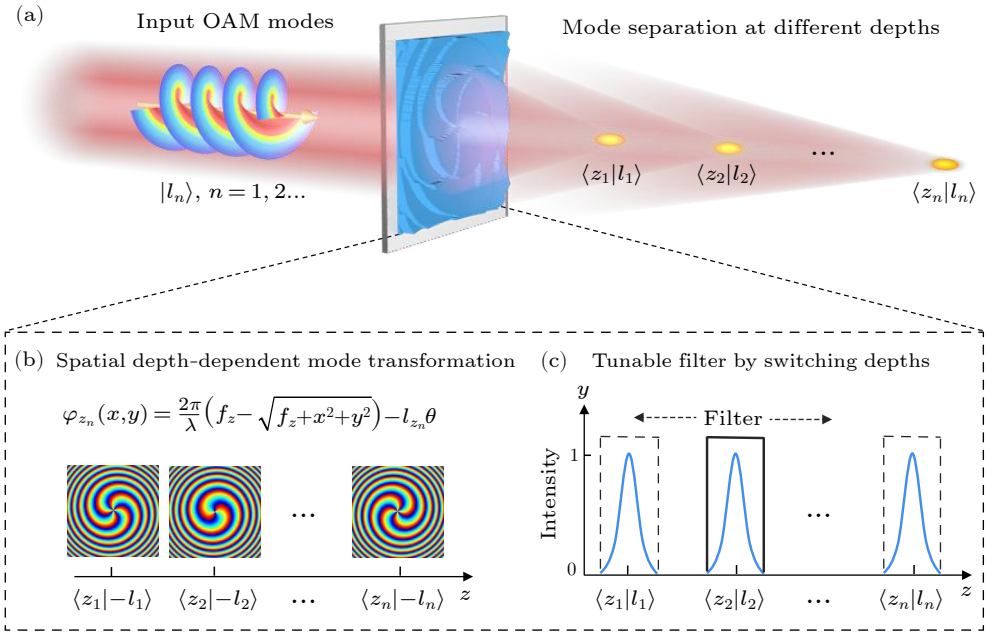

Fig. 1. Schematic of spatial depth-dependent mode transformation. (a) Operating principle of tunable filtering, which maps input orbital angular momentum (OAM) modes into Gaussian modes at varying spatial depths. (b) Design principle of spatial depth-dependent mode transformation that integrates the spiral phase and lens phase. (c) Intensity profiles of the filtered modes as a function of spatial depth.

A schematic illustrating the mechanism of the spatial-depth-dependent mode transformation is shown in Fig. 1(a). Using this transformation, the input modes (l_n, $n = 1, 2, \ldots$) are individually demultiplexed into Gaussian modes positioned at distinct depth planes (Z_m, $m = 1, 2, \ldots$). The core of this transformation lies in the integration of the spiral and lens phases, which can demultiplex the OAM mode and focus on a pre-designed diffraction distance. Thus, at a certain axial distance, the phase shift can be mathematically expressed as follows:

$$\varphi(x, y) = 2\pi/\lambda(f - \sqrt{f^2 + x^2 + y^2}) - l\theta, \qquad (1)$$

where (x, y) represents the Cartesian coordinates, f is the focal length of the lens phase, and θ is the azimuthal angle. Based on the conservation of OAM, only the input OAM mode with a topological charge l is converted into the Gaussian mode at a predetermined diffraction distance f, whereas the other modes retain their characteristic doughnut-shaped intensity distribution. The difference in spatial intensity distribution between the Gaussian and OAM modes allowed us to efficiently separate the target Gaussian modes through the circular aperture. To achieve independent mapping between the different incident OAM modes and axial depths, we positioned distinct modes at discrete spatial depths, as depicted in Fig. 1(b). In addition, weight factors were introduced for each diffraction order to ensure a uniform energy distribution of the modes across different spatial depths. Numerical optimization using a simulated annealing algorithm was then performed to derive the final phase profile:

$$\psi(x, y) = \arg\left\{\sum_{q=1}^{Q} C_q e^{i\varphi_q(x, y)}\right\}, \qquad (2)$$

where $\psi(x, y)$ represents the spatial depth-mode transformation phase, q is the diffraction order ranging from 1 to Q, and C_q is the weight factor of the q diffraction order. Equation (1) can be expressed as $\varphi_q(x, y) = 2\pi/\lambda(f_q - \sqrt{f_q^2 + x^2 + y^2}) - l_q\theta$. Through the spatial depth–mode transformation, the incident OAM modes are demultiplexed into Gaussian modes and separated at different diffraction distances. By leveraging the difference in spatial energy distribution between the Gaussian and OAM modes and adjusting the filtering position at various

spatial depths, selective filtering of arbitrary coaxially incident OAM mode channels can be achieved, as illustrated in Fig. 1(c).

The TPL technique[28,29] is a high-resolution lithography method that enables the rapid fabrication of three-dimensional (3D) freeform structures in a single manufacturing step with precise lateral and azimuthal resolutions. Utilizing this technique, we designed polymerized resin pillars on a SiO_2 substrate with a lattice period of 4 μm, achieving phase modulation by adjusting the relative height H of the pillars, as illustrated in Fig. 2(a). Finite-difference time-domain (FDTD) simulations were employed to investigate the phase variations and amplitude responses of the pillars at different heights. As shown in Fig. 2(b), the phase variation covers the entire 0 to 2π range as the relative height varies from 0 to 3.1 μm, while maintaining a high transmission amplitude (>0.8). By correlating the phase value of each pixel in the pre-designed phase pattern with the corresponding pillar height, the spatial depth-dependent mode transformation phase can be encoded onto the fabricated sample. To validate the feasibility of this approach, we fabricated a mode filter based on TPL, encoding five OAM modes (l = 0, ±2, ±4) at discrete spatial depths ranging from 13.5 to 39 mm. Scanning electron microscopy (SEM) images of the fabricated filter at different magnifications are shown in Fig. 2(c). The fabrication procedure is described in detail in Supplementary Note 1.

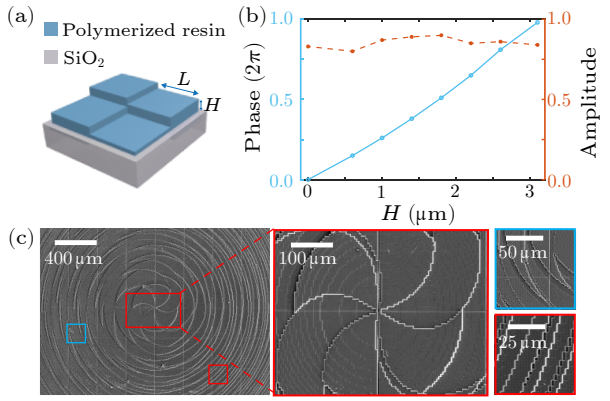

Fig. 2. Design and realization of the mode filtering. (a) Schematic of nanopillars arranged on a glass substrate. (b) Diagram depicting the variation in phase and amplitude of the pillars as a function of height. (c) Scanning electron microscope (SEM) images of the fabricated mode filter.

The optical performance of the proposed filter was characterized using a custom-built optical setup. A 1550 nm Gaussian beam was normally incident on the filter, and the resulting output light field was collected by an objective lens and recorded by a charge-coupled device (CCD) camera (see details of the experimental setup in Supplementary Note 2). To investigate the mode evolution during transmission experimentally, the topological charges were detected using the diffraction pattern produced by a cylindrical lens (C-lens). The topological charge of the OAM mode can be identified by the number and orientation of the diffraction stripes. As shown in Fig. 3, with increasing transmission distance, the topological charge of the output light field sequentially transforms from −4 to −2, 0, +2, +4, accompanied by the corresponding changes in the beam radius. This indicates that the OAM mode carried by the output light field is continuously converted with the transmission distance, demonstrating the feasibility of spatial depth-dependent mode transformation.

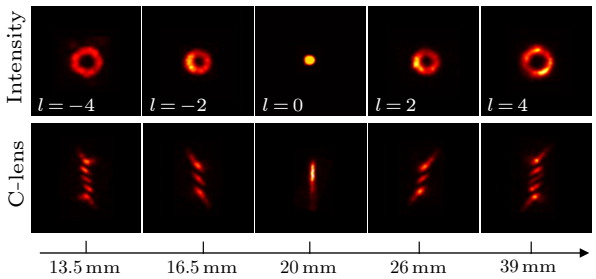

Fig. 3. Measured transverse profiles of the output beam at various planes along the propagation direction, along with the corresponding detected results.

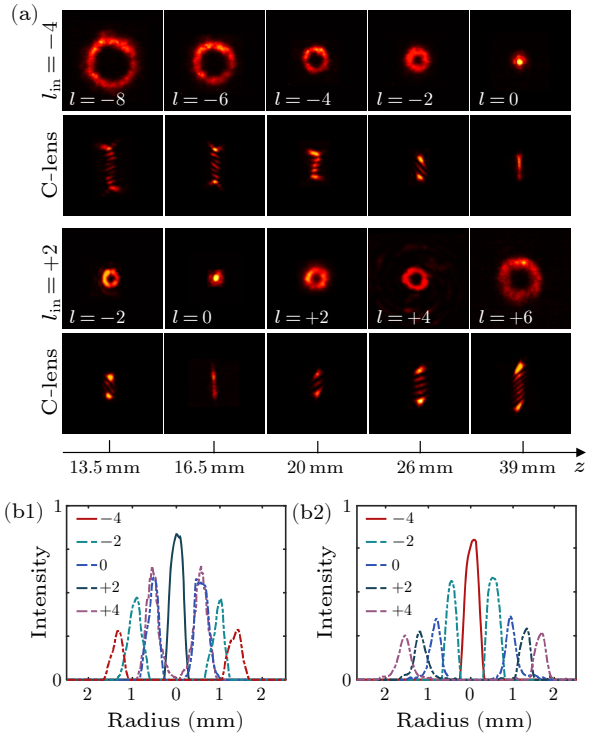

Fig. 4. Experimental results of different incident OAM modes after spatial-depth separation and mode conversion. (a) Output optical field distribution at various axial spatial distances after spatial depth–mode conversion for incident OAM modes (l_{in} = −4, +2), along with the corresponding detection results. The topological charges of different output optical fields are labeled in the bottom left corner. (b1, b2) Lateral intensity distribution of the focused optical field at z = 16.5 mm and z = 39 mm.

Subsequently, we experimentally validated the mode filter performance using various incident OAM modes (l_{in} = 0, ±2, ±4). Figure 4(a) illustrates the intensity distribution of the output light at varying transmission

depths after two distinct incident OAM modes ($l_{\text{in}} = -4$, $+2$) are passed through the proposed mode filter. The results indicate that at a consistent transmission depth, only one input mode is successfully reconverted into a Gaussian mode, whereas the remaining modes are transformed into other OAM modes characterized by doughnut-shaped intensity distributions (additional results with different input modes are provided in Supplementary Note 3). Statistical analysis of the lateral intensity distribution of the different modes at the same axial spatial distance was performed. Figures 4(b1) and 4(b2) correspond to transmission depths of $z = 16.5$ and 39.5 mm, respectively. The results demonstrate that the input modes are effectively separated at different transmission distances, highlighting the efficacy of this mode-filtering scheme, which utilizes the difference in intensity distribution between the Gaussian and OAM modes to isolate the Gaussian mode. Finally, to qualitatively assess the filtering performance of the proposed scheme, we measured the crosstalk data across different channels, as depicted in Fig. S3. The average crosstalk was found to be below −10.9 dBm, demonstrating excellent filtering performance.

As a proof of concept, we developed a five-channel OAM mode-multiplexing communication system and selectively filtered arbitrary channels using the proposed mode filter, as detailed in Supplementary Note 5. In this experimental setup, five collimated Gaussian beams, each carrying 50 Gbit/s QPSK signals, were incident at a specific angle onto our previously proposed OAM multiplexing device, which is based on Dammann vortex gratings.[30,31] Through off-axis phase modulation, the incident beams were redirected into coaxially transmitted vortex beams for OAM multiplexing, with topological charges of 0, ±2, and ±4. These multiplexed vortex beams were then directed perpendicularly onto the filter, which was encoded by a spatial depth-dependent mode transformation phase. Consequently, each multiplexed vortex beam was diffracted and converted into an axial Gaussian focal spot at distinct axial depths. By selectively filtering and collimating the Gaussian focal spot at a specific axial depth using an aperture and lens, the paralleled Gaussian beam was coupled to a single-mode fiber for demodulation. Figure 5(a) presents the measured BERs of the five multiplexed channels as functions of the received power. The red dashed line represents the forward error correction (FEC) threshold. All BER values remained below the FEC threshold of 3.8×10^{-3} when the received power was below −23 dBm. When the received power reached −16 dBm, the BERs approached zero. Figure 5(b) shows the constellation diagrams of two OAM channels at the received power of −16 and −23 dBm, respectively. The constellation diagrams of the different channels exhibit similar patterns and significant convergence at various power levels, indicating excellent communication performance. Furthermore, this approach can be combined with polarization-division multiplexing by leveraging the polarization-independent characteristics of the mode filter. The communication performance was experimentally assessed, as detailed in Supplementary Note 6, demonstrating BERs below 10^{-6} at a received optical power of −16 dBm. These results underscore the superior selective demultiplexing performance of the fabricated filters.

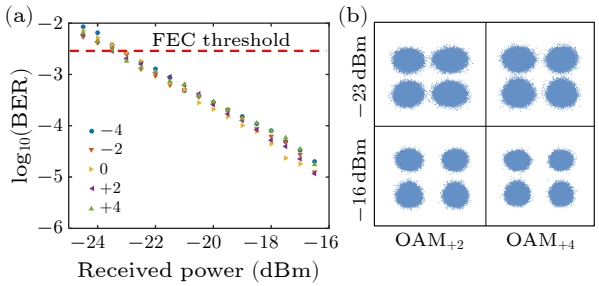

Fig. 5. Communication results of selective demultiplexing using the proposed mode filter. (a) Measured mode bit error rate (BER) for five OAM mode channels. (b) Constellation diagrams for different channels at varying optical power levels.

Exploiting the inherent independence of the spatial depth and mode, our approach exhibits significant flexibility in separating coaxially transmitted OAM modes, thereby facilitating selective mode filtering. To illustrate this capability, we reestablished the depth–mode mapping relationship and demonstrated the selective filtering of seven OAM modes ($l = -3,\ 0,\ 2,\ -5,\ -1,\ 6,\ 3$) with varying mode intervals, as presented in Supplementary Note 7. The results indicated that the input Gaussian beam was sequentially converted into seven independent OAM modes while maintaining a uniform light intensity distribution. Moreover, to enhance information transmission efficiency, the angle dimension can be further incorporated to construct one-to-many multicast communication links (Supplementary Note 8). By integrating the angle separation mechanism of Bragg gratings,[32] the output light can be equally divided into different 3D diffraction orders, enabling receivers with different diffraction orders to download the target channels by independently adjusting the spatial depth. However, the number of multiplexing orders affects the energy efficiency of mode filters. Therefore, a balance between the number of orders and energy utilization should be considered in practice.

In summary, we proposed and implemented a tunable mode filtering technique based on a spatial depth-dependent mode transformation. By integrating the spiral and lens phases, multiplexed OAM modes can be mapped to different spatial depths, thereby enabling mode separation and demultiplexing. This approach allows tunable mode filtering by adjusting the spatial depths. In our experiments, we successfully separated five OAM modes at spatial depths ranging from 13.5 to 39 mm, with an average mode crosstalk below −10.9 dBm. Additionally, we constructed a five-channel OAM mode-multiplexing communication system, wherein arbitrary channels could be selectively demultiplexed, achieving the transmission of 250 Gbit/s QPSK signals with BERs below 10^{-6} at a received power of −16 dBm. This spatial depth-dependent filtering strategy is expected to overcome the challenges associated with the selective separation of OAM modes and holds significant potential for establish-

ing mode-multiplexing communication networks and facilitating channel interconnections.

Acknowledgements. This work was supported in part by the National Natural Science Foundation of China (Grant No. 6227132), the Basic and Applied Basic Research Foundation of Guangdong Province (Grant No. 2023A1515030152), the Science and Technology Program of Shenzhen (Grant No. JCYJ20210324095610027), the Natural Science Foundation of Top Talent of SZTU (Grant No. GDRC202204), the Science and Technology Project of Shenzhen (Grant No. ZDSYS201707271014468). The authors also acknowledge the technical assistance from the Photonics Research Centre of Shenzhen University.

References

[1] Wang J, Liu J, Li S, Zhao Y, Du J, and Zhu L 2022 *Nanophotonics* **11** 645
[2] Chen J, Wan C, and Zhan Q 2021 *Adv. Photonics* **3** 064001
[3] Li Y, Li X, Chen L W, Pu M B, Jin J J, Hong M H, and Luo X G 2017 *Adv. Opt. Mater.* **5** 1600502
[4] Liu Z B, Gao S C, Lai Z Y, Li Y R, Ao Z H, Li J P, Tu J J, Wu Y X, Liu W P, and Li Z H 2023 *Laser Photonics Rev.* **17** 2200536
[5] Fang Z Y, Xu H F, Zheng Y Q, Chen Y L, and Zhou Z K 2020 *Chin. Phys. Lett.* **37** 077801
[6] Noguchi Y, Nakayama S, Ishida T, Saitoh K, and Uchida M 2019 *Phys. Rev. Appl.* **12** 064062
[7] Tan H Y, Deng J H, Zhao R Z, Wu X, Li G X, Huang L L, Liu J, and Cai X L 2019 *Laser Photonics Rev.* **13** 1800278
[8] Sahu R, Chaudhary S, Khare K, Bhattacharya M, Wanare H, and Jha A K 2018 *Opt Express* **26** 8709
[9] Guo Y, Zhang S, Pu M, He Q, Jin J, Xu M, Zhang Y, Gao P, and Luo X 2021 *Light Sci. Appl.* **10** 63
[10] Leach J, Courtial J, Skeldon K, Barnett S M, Franke-Arnold S, and Padgett M J 2004 *Phys. Rev. Lett.* **92** 013601
[11] Babazadeh A, Erhard M, Wang F, Malik M, Nouroozi R, Krenn M, and Zeilinger A 2017 *Phys. Rev. Lett.* **119** 180510
[12] Wang F, Erhard M, Babazadeh A, Malik M, Krenn M, and Zeilinger A 2017 *Optica* **4** 1462
[13] Huang H, Ren Y X, Xie G D, Yan Y, Yue Y, Ahmed N, Lavery M P J, Padgett M J, Dolinar S, Tur M, and Willner A E 2014 *Opt. Lett.* **39** 1689
[14] Lin Z, Xie Z, He Y, Wang X, Wu H, Wang S, Guan Z, Liu J, Ye H, Li Y, Fan D, and Chen S 2021 *Opt. Lett.* **46** 5563
[15] Fang J C, Xie Z W, Lei T, Min C J, Du L P, Li Z H, and Yuan X C 2018 *ACS Photonics* **5** 3478
[16] Hao Z, Zhu S, Qiu C W, Xu Y, and Chen H 2024 *Chin. Opt. Lett.* **22** 033601
[17] Li J, Li J, Yue Z, Zheng C, Wang G, Liu J, Xu H, Song C, Yang F, Li H, Li F, Tang T, Zhang Y, Zhang Y, and Yao J 2022 *Laser Photonics Rev.* **16** 2200325
[18] Lu Z C, Deng Y H, Yu Y, Huang C Z, and Yang J B 2023 *Chin. Phys. Lett.* **40** 114201
[19] Huang Z, He Y, Wang P, Xiong W, Wu H, Liu J, Ye H, Li Y, Fan D, and Chen S 2022 *Opt. Express* **30** 5569
[20] Wang Y, Yao Z Y, Cui Z J, Sun G C, and Zhang D C 2023 *Nanophotonics* **12** 4339
[21] Huang L L, Chen X Z, Mühlenbernd H, Zhang H, Chen S M, Bai B F, Tan Q F, Jin G F, Cheah K W, Qiu C W, Li J, Zentgraf T, and Zhang S 2013 *Nat. Commun.* **4** 2808
[22] Fang X Y, Ren H R, and Gu M 2020 *Nat. Photonics.* **14** 102
[23] Bi Y, Huang L, Li T, Wang C, Zou X, Zhou L, and Kang G 2024 *Chin. Opt. Lett.* **22** 043601
[24] Dorrah A H, Rubin N A, Tamagnone M, Zaidi A, and Capasso F 2021 *Nat. Commun.* **12** 6249
[25] He X, Bao H, Zhang F, Kang T, Pu M, Chen Y, Guo Y, Gong J, Xu M, and Luo X 2024 *Nanophotonics* **13** 1657
[26] Dorrah A H, Rubin N A, Zaidi A, Tamagnone M, and Capasso F 2021 *Nat. Photonics* **15** 287
[27] Xu P F, Tong X, Zeng Z S, Liu S X, and Zhao D M 2024 *Chin. Phys. Lett.* **41** 074201
[28] Goi E, Schoenhardt S, and Gu M 2022 *Nat. Commun.* **13** 7531
[29] Goi E, Chen X, Zhang Q, Cumming B P, Schoenhardt S, Luan H, and Gu M 2021 *Light Sci. Appl.* **10** 40
[30] Chen S, Xie Z, Ye H, Wang X, Guo Z, He Y, Li Y, Yuan X, and Fan D 2021 *Light Sci. Appl.* **10** 222
[31] Zeng Q, Wang J, Huang H, Wu H, Ren J, Nong L, Xie Z, Liu J, Ye H, and Fan D 2023 *Opt. Express* **31** 42299
[32] Liu S J, Chen P, Ge S J, Zhu L, Zhang Y H, and Lu Y Q 2022 *Laser Photonics Rev.* **16** 2200118